Aquaculture 453 (2016) 1–9

Contents lists available at ScienceDirect

Aquaculture

journal homepage: www.elsevier.com/locate/aquaculture

Pathology and physiology of *Haliotis diversicolor* with withering syndrome

Guilan Di [a,b], Xianghui Kong [a], Guorong Zhu [a], Shengli Liu [a], Chao Zhang [a], Caihuan Ke [b,*]

[a] College of Fisheries, Henan Normal University, Xinxiang 453007, China
[b] State Key Laboratory of Marine Environmental Science, College of Ocean and Earth Sciences, Xiamen University, Xiamen, China

ARTICLE INFO

Article history:
Received 4 September 2015
Received in revised form 18 November 2015
Accepted 19 November 2015
Available online 26 November 2015

Keywords:
Haliotis diversicolor
Withering syndrome
Ultrastructural lesions
Mucus enzymatic activities
2-DE
SDS-PAGE

ABSTRACT

Abalone withering syndrome is a serious chronic disease. Ultrastructure and pathological changes were studied using transmission electron microscopy. Myofibers appeared hollow, and the number of inner intact myofibrils was reduced greatly. The morphology of mitochondria in cells appeared abnormal. Crystal lattice-like inclusions in pathological muscle cells were observed. The hepatopancreas was damaged severely; it was full of empty vesicles and devoid of any recognizable cellular structures. The activities of 3 enzymes, acid phosphatase (ACP), alkaline phosphatase (AKP), and total superoxide dismutase (T-SOD), in hemolymph of healthy and diseased abalone showed little differences. ACP activity in the pedal mucus of healthy and diseased abalone was not significantly different. However, in diseased abalone pedal mucus, activities of AKP and T-SOD were significantly lower than in the control group. In pedal mucus of healthy and diseased abalone, the differential (SDS-PAGE) bands were identified as actin and hemocyanin. Protein identification was accomplished with mass spectrometry. A total of 16 2-DE gel spots were identified; 5 gel spots showed upregulation and 11 gel spots showed downregulation in diseased abalone. Proteins involved in energy production and storage, including fructose-1, 6-bisphosphate aldolase, arginine kinase, and triosephosphate isomerase, showed diverse expression patterns in diseased abalone. For stress-responsive proteins, expression of Cu/Zn-superoxide dismutase showed downregulation. For contraction and regulation proteins of muscle, actin showed significant downregulation.

Statement of relevance: Abalone withering syndrome (WS) is a serious chronic disease. However, there is limited information on the physiological performance of infected abalones. The present study was to assess the alterations of *Haliotis diversicolor* caused by WS using transmission electron microscopy as well as assess the immune enzyme activity of hemolymph and mucus, and muscle, mucus proteins changes by 2-DE and SDS-PAGE.

1. Introduction

Abalone (Haliotis spp.) is a marine gastropod that is distributed worldwide along coastal waters in tropical and temperate areas and is an economically important seafood (Li and Yan, 2010). The small abalone, *Haliotis diversicolor*, is a commercially important species cultured along the coast of southern China (Cai and Wang, 2008). China, with more than 50,000 tons per annum (Di et al., 2013), is the most important abalone-producing country in the world. Since 1999, the yields of cultured abalone in China have been severely affected by continual outbreaks of a fatal epidemic disease caused by abalone withering syndrome. Withering syndrome is a serious chronic disease that affects various abalone species in both natural and farmed populations. It was first observed in the 1980s in the Channel Islands southwest of California, where it caused a 99% decline in the population of the black abalone (*Haliotis cracherodii*). Since then, it has been detected in pink (*Haliotis corrugata*), flat (*Haliotis walallensis*), white (*Haliotis sorenseni*), red (*Haliotis rufescens*), green (*Haliotis fulgens*), Taiwanese (*H. diversicolor supertexta*) abalones, as well as in *Haliotis tuberculata* and *Haliotis discus hannai* (Wetchateng et al., 2010; Crosson et al., 2014).

Withering syndrome is caused by infection with the intracellular rickettsial bacterium *Candidatus Xenohaliotis californiensis* (a *Rickettsia*-like organism) (Rosenblum et al., 2008; Crosson et al., 2014; Friedman et al., 2014). Withering syndrome occurs along the eastern Pacific margin of North America in California, USA, and Baja California, Mexico, and abalones in Chile, China, Taiwan, Iceland, Ireland, Israel, Spain, Thailand and Japan have been also infected (Crosson et al., 2014).

Gross signs of the disease include pedal atrophy, a mottled digestive gland, anorexia, weakness, and lethargy (Gardner et al., 1995; Friedman et al., 2000, 2002; Balseiro et al., 2006). Moribund abalones have less elasticity and melanization of the mantle and muscle with recessive feeding, and most fall from the reef and die (Zhuang et al., 2010; Jiang

* Corresponding author at: College of Ocean and Earth Sciences, Xiamen University, Xiamen 361005, PR China.
E-mail address: chke@xmu.edu.cn (C. Ke).

http://dx.doi.org/10.1016/j.aquaculture.2015.11.030
0044-8486/

et al., 2012). Withering syndrome is manifested by morphological changes in the digestive gland, which yields a loss of functionality. The distribution, impacts, current diagnostic methods, and new findings about abalone withering syndrome have been reviewed (Crosson et al., 2014). It is important to determine the effects of withering syndrome on the physiological performance of abalone. However, there is no such information available (González et al., 2012).

Functional proteomics have become a powerful tool for the identification of sample proteins differentially responding to microorganisms or special stimuli. Use in marine invertebrates is limited and few proteomic analysis studies have been conducted in *H. diversicolor* with withering syndrome. The epidermal mucus is considered an important component of innate immunity. In addition, acid phosphatase (ACP) and alkaline phosphatase (AKP) are important for innate immune defense in small abalone (Wang et al., 2004). Superoxide dismutase (SOD) is an important antioxidant.

This article examines the effects of withering syndrome on the physiological performance of abalone. Alterations of *H. diversicolor* caused by withering syndrome were studied using transmission electron microscopy (TEM), enzyme activities, and 2-dimensional gel electrophoresis.

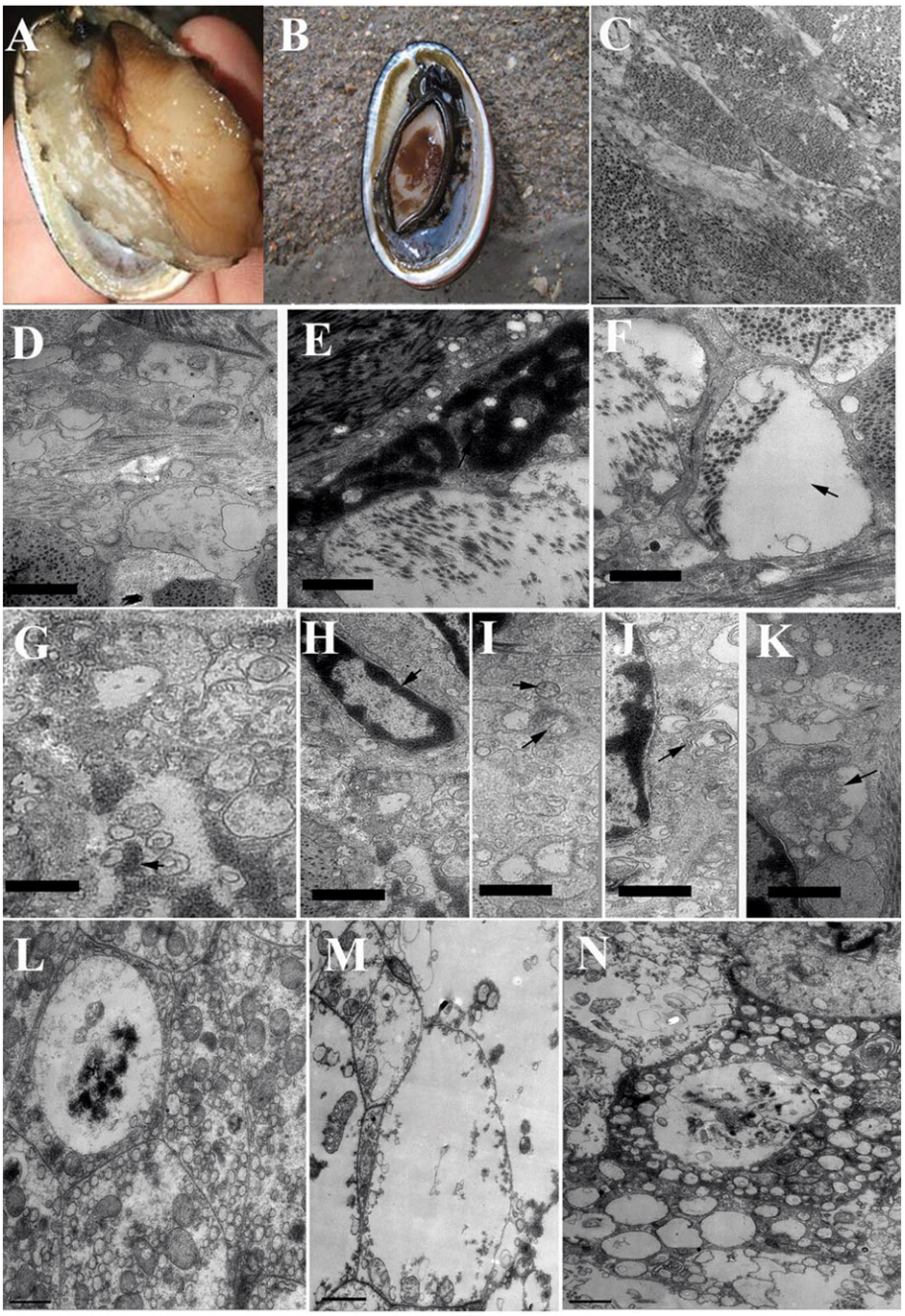

Fig. 1. (A): Healthy small abalone (*Haliotis diversicolor*). (B): Withering syndrome in a small abalone (*H. diversicolor*). (C): Electron microscopy of an abalone with a healthy pedal, the bar = 1 μm. (D–K): Pathological changes in the foot of abalone (*H. diversicolor*) with amyotrophia, the bar = 1 μm. (D): Foot tissue cells were devoid of intracellular organelles and cell components disappeared. (E): Like-inclusions appeared in the nucleus. (F, G): Myofibers appeared hollow, and the number of inner intact myofibrils was obviously reduced (arrow). (H): Karyoplasm gathered at the edge of the nucleus in the foot cells (arrow). (I): Morphology of mitochondria in muscle cells was abnormal and crystal lattice-like inclusion bodies appeared (arrow). (J): The structure of foot cells appeared myelin-like (arrow). (K): Tubular structures proliferated in the foot cells, and the foot cells were full of empty vesicles (arrow). L–N: Pathological changes of the hepatopancreas in abalone (*H. diversicolor*) with amyotrophia, the bar = 1 μm. (L): The hepatopancreas in a healthy abalone. (M): The number of mitochondria greatly decreased. (N): The cells were full of empty vesicles and devoid of any recognizable cellular structures.

Samples from the mucus, muscle, and hemolymph of healthy and infected abalone were investigated.

2. Materials and methods

2.1. Sample collection

Eighteen diseased small abalones (shell length of 3.95 ± 0.19 cm, about 9 months after fertilization) with withering syndrome and 18 healthy abalones were collected separately from abalone farms (Dongshan Haitian Aquaculture Co., Ltd., Fujian Province, China). Each abalone was assessed as either a healthy abalone with a foot and viscera that filled the entire shell volume or a diseased abalone with severe atrophy of the foot muscle (Fig. 1A, B).

2.2. TEM sample preparation

Tissues of control and diseased small abalone were fixed with 2.5% glutaraldehyde in PBS for 3 h at 4 °C, pH 7.4, and were then fixed in 1% osmium tetraoxide at room temperature for 2 h. After eliminating remaining glutaraldehyde and osmium tetraoxide, the dehydration process was conducted with, 50, 70, 80, 95, and 100% ethanol. The fixed samples were embedded with Epon and they were then cut into smaller samples with an ultramicrotome (Leica Ultracut). Ultrathin sections were cut at 80-nm thickness and post-stained with 2% uranyl acetate and 1% lead citrate for examination under TEM. The sections were photographed with a JEM-2100EX transmission electron microscope.

2.3. Assessment of immune parameters in abalone

2.3.1. Collection of pedal mucus and hemolymph

Mucus: Sterile glass slides were used to collect mucus from the pedal surface of abalone. The abalones were put on clean glass slides (about 3 abalone per slide) and allowed to crawl for 1 h. Then, the animals were removed, and, after addition of a small volume of sterile PBS, the pedal mucus was carefully scraped from the glass slides. To obtain a pure mucus fraction, the samples were centrifuged (14,000 ×*g*, 15 min, 4 °C) and filter-sterilized (0.45 μm membrane). The samples of mucus proteins were aliquoted and stored at −80 °C.

One milliliter hemolymph samples were collected using a capillary tube to withdraw fluid from a central incision in the pedal muscle. The samples were transferred into a 1.5 mL centrifuge tube and immediately centrifuged at 2000 ×*g* for 10 min (4 °C) to remove the hemocytes. The supernatant was frozen at −80 °C until used.

2.3.2. Assessment of enzymatic activities

Assays of enzymatic activities were performed using a standard assay kit from the Nanjing Jiancheng Bioengineering Institute (Nanjing, China) and following the manufacturer's instructions. Enzymatic activities were determined spectrophotometrically (BIO-RAD 680). Protein concentration was determined using the Coomassie Brilliant Blue (G-250) method described by Bradford, with bovine serum albumin as a standard. Enzyme activities were expressed as units per milligram of protein (U/mg protein).

Total SOD (T-SOD) activity was assayed using the xanthine–xanthine oxidase method. The assay was conducted in a 96-well microplate, where hemolymph or mucus was added to xanthine–xanthine oxidase reagent and incubated for 40 min at 37 °C. SDS was then added to stop the reaction, and absorbance at 550 nm was determined. One unit of SOD was defined as the amount of SOD inhibiting the rate of reaction by 50% per mL of hemolymph or mucus.

ACP and AKP activity were determined spectrophotometrically at 520 nm using disodium phenyl phosphate as a substrate. Hemolymph or mucus was added to the reactive substrate and incubated at 37 °C for 30 min for ACP and 15 min for AKP. One unit of activity was defined as the amount of enzyme required to transform 1 mg of phenol in the reactive substrate (disodium phenyl phosphate) at 37 °C, and activity was expressed as U/mg protein.

2.3.3 Statistical analysis

All statistical analyses were performed with SPSS program version 17.0 (SPSS, Chicago, IL, USA). An independent sample T-test was conducted to explore whether enzymatic activities in healthy and diseased abalone groups were significantly different. A probability (p) value of less than 0.05 was considered significant.

2.4. Analysis of pedal mucus of healthy and diseased abalone with SDS-PAGE electrophoresis

Samples were separated with SDS-PAGE on a BIO-RAD electrophoresis unit. Discontinuous electrophoresis was conducted with a 12.5% running gel and a 4% stacking gel. A sample of 30 μg and molecular weight standards was loaded in each of several wells on the gel. All of the samples were then mixed in a 1:1.5 ratio with the sample buffer (4.6% SDS, 10% β-mercaptoethanol, 20% glycerol, 1.5% Tris, 1% bromophenol blue) and heated to 60 °C for 15 min. They were then cooled. Then, 20 μL aliquots were used for SDS-PAGE. SDS-PAGE was carried out at a constant current of 10 mA per gel for 3 h, followed by 15 mA per gel until the tracking dye (bromophenol blue) had migrated to the bottom of the gel. The gel was stained using Coomassie brilliant blue (CBB).

2.5. Two-dimensional gel electrophoresis (2-DE) and analysis

2.5.1. Abalone pedal muscle protein extraction

Twenty mg of muscle powder was suspended in 1 mL of TRIzol. Abalone pedal muscle protein extraction was performed as previously described (Di et al., 2013, 2015). The dry pellet was resuspended using isoelectric focusing (IEF) re-dissolving buffer (7 M urea, 2 M thiourea, 40 mM Tris, 4% [*w*/*v*] CHAPS). Protein quantification in the urea-containing protein samples was measured according to the method of the Protein 2-D Quant kit (GE Healthcare, USA). The samples obtained from 18 diseased abalones or 18 healthy abalones were divided into 3 subgroups, each containing 6 abalone muscles to yield 120 μg protein per subgroup, which was stored at −70 °C.

2.5.2. 2-DE

The protein sample was mixed with a rehydration buffer [8 M urea, 2% (*w*/*v*) CHAPS, 20 mM DTT, 0.5% (*v*/*v*) IPG buffer (pH 4–7), and 0.01% (*w*/*v*) bromophenol blue] before being loaded onto IPG strips with a linear pH gradient of 4–7 (Amersham Pharmacia Biotech, Piscataway, USA) in a horizontal electrophoresis apparatus (Bio-Rad). The sample was subjected to isoelectric focusing in the following manner: 13 h at 50 V (active rehydration), 100 V for 2 h, 200 V for 2 h, 500 V for 1 h, 1000 V for 2 h, 4000 V for 2 h, and 50,000 Vh at 8000 V.

Subsequently, immobilized pH gradient strips were gently soaked for 17 min in equilibration solution containing 6 M urea, 2% SDS, 50 mM Tris–Cl (pH 8.8), 30% glycerol, and 1% DTT, followed by equilibration for 17 min in equilibration solution containing 6 M urea, 2% SDS, 50 mM Tris–Cl (pH 8.8), 30% glycerol, and 2.5% iodoacetamide. Two-dimensional SDS-PAGE gels were carried out on 12.5% polyacrylamide gels (20 cm × 20 cm × 1.5 mm) in a PROTEAN xi cell (Bio-Rad) at 12.5 mA/gel for 30 min and then 25 mA/gel for ~6 h. The 2-DE gels were visualized using silver nitrate, while preparative gels were stained using CBB. The 2-D gels were scanned using an Image Scanner (Amersham Biosciences, UTA-1100), and spot intensity differences were analyzed using the PDQuest 8.0 software package (Bio-Rad).

Differentially expressed proteins were identified as having a spot intensity difference of at least 1.5-fold between diseased abalones and healthy abalones. For qualitative analysis, spot intensities with at a least a 10-fold change were considered present/absent.

2.6. In-gel protein digestion

For identification, stained gel pieces and sections of SDS-PAGE were excised. The excised stained gel pieces and SDS-PAGE sections were washed with 200 μL of Milli-Q H_2O 3 times for 6 min each. The spots were shaken in 200 μL of 25 mM NH_4HCO_3 solution for 20 min, dehydrated with 200 μL acetonitrile (ACN) for 12 min and then air-dried at room temperature. The proteins were reduced with 10 mM DTT for 30 min at 56 °C and alkylated with 55 mM iodoacetamide (IAA). All gel pieces were incubated with 12.5 ng/μL trypsin in 10 mM NH_4HCO_3 overnight at 37 °C.

2.7. Protein identification by mass spectrometry (MS) and database search

The proteins were identified using MALDI-TOF/TOF with a 5800 Proteomics Analyzer (Applied Biosystems). For MALDI-TOF/TOF, after digestion, peptides were extracted from the gel pieces using 5 μL of 50% (*v*/*v*) ACN and 0.1% (*v*/*v*) trifluoroacetic acid (TFA). The peptide solution was transferred to the target plate. Next, 0.8 μL of the peptide solution was mixed with 0.4 μL of matrix solution (2 μg/μL α-cyano-4-hydroxycinnamic acid) in 50% (*v*/*v*) ACN and 0.1% (*v*/*v*) TFA. The target well was covered and allowed to air dry. The major peaks obtained from MALDI-TOF were selected for further tandem mass spectrometry (MS/MS) analyses. Spectra were submitted for database comparison with the MASCOT search engine. The MASCOT search of the MS data was performed against the non-redundant National Centre for Biotechnology Information (NCBI, USA) database using the following search parameters: enzyme (trypsin), up to one missed cleavage, fixed modification, carbamidomethylation (C) and variable modification, oxidation (M), monoisotopic mass values, protein mass unrestricted, peptide mass tolerance ±200 ppm, and fragment mass tolerance ±1 Da.

2.8. De novo sequencing

First, DeNovo Explorer software (AB SCIEX) was used for *de novo* sequencing. Each MS/MS spectrum produced 10 peptide sequences and each peptide sequence received a score. In order to minimize randomness, only those peptides with a score higher than 95 were considered in this study (Wang et al., 2011).

Second, some proteins were not identified using DeNovo Explorer software. Then, *de novo* peptide sequences were used for homology searches using MS-BLAST. MS-BLAST searches were conducted via the Washington University server (http://genetics.bwh.harvard.edu/msblast/). The search results were considered significant if the resulting scores were higher than the threshold score. However, only high-scoring segment pairs (HSSPs) with a score of 62 or above were considered (Wang et al., 2011).

3. Results

3.1. Ultrastructural pathological changes

Compared with healthy abalones (see Fig. 1A), abalones with withering syndrome were characterized by atrophied pedal musculature, mantle retraction, epipodial discoloration, and diminished responsiveness to tactile stimuli, ultimately preventing the animal from feeding effectively and causing malabsorption of food, weakness, lethargy, constriction of body mass, and finally death (see Fig. 1B).

Electron micrographs of ultrathin sections of healthy muscle tissue revealed tightly arranged and regular structures (see Fig. 1C). Compared with normal tissue, ultrastructure of diseased muscle cells showed obvious and typical pathological changes (see Fig. 1D–K). Muscle fibers were disorderly arranged and fiber arrangement became loose, and some muscle fibers showed focal necrosis; myofibers appeared hollow, and the number of inner intact myofibrils was obviously reduced (see Fig. 1D, F, G). There were different inclusions in the nucleus of some damaged cells (see Fig. 1E). The nucleoplasm gathered at the edge of the nucleus in diseased abalone muscle cells, and the electron density of nucleoplasm at the edge of the nucleus was particularly high (see Fig. 1H), indicating irreparable injury of the nucleus and cell death. A common form of mitochondrial damage and the result of mitochondrial membrane damage is the formation of myelin-like layered structures. In addition, pathological inclusions could be observed in the mitochondrial matrix or cristae. The morphology of mitochondria in diseased cells was abnormal, and crystal lattice-like inclusions in pathological muscle cells could be observed (see Fig. 1I). Cell membranes appeared as spiral or concentric layered structures when cell membranes had serious injury, forming typical myelin-like structures (see Fig. 1J). Tubular structures increased greatly (see Fig. 1K). These results showed that the muscle tissue was highly damaged.

The hepatopancreases were damaged the most: they were filled with empty vesicles and devoid of any recognizable cellular structures (see Fig. 1L–N). The number of mitochondria had greatly decreased (Fig. 1M).

3.2. AKP, ACP, and SOD activity

Overall, enzyme activities of ACP, AKP and T-SOD in the hemolymph of healthy and diseased abalone showed little differences ($p > 0.05$) (see Fig. 2A). Although there were no significant differences between all 3 enzyme activities in the hemolymph of diseased abalone compared with healthy abalone, there was a measureable decrease in AKP activity and a slight increase in T-SOD and ACP within diseased abalone.

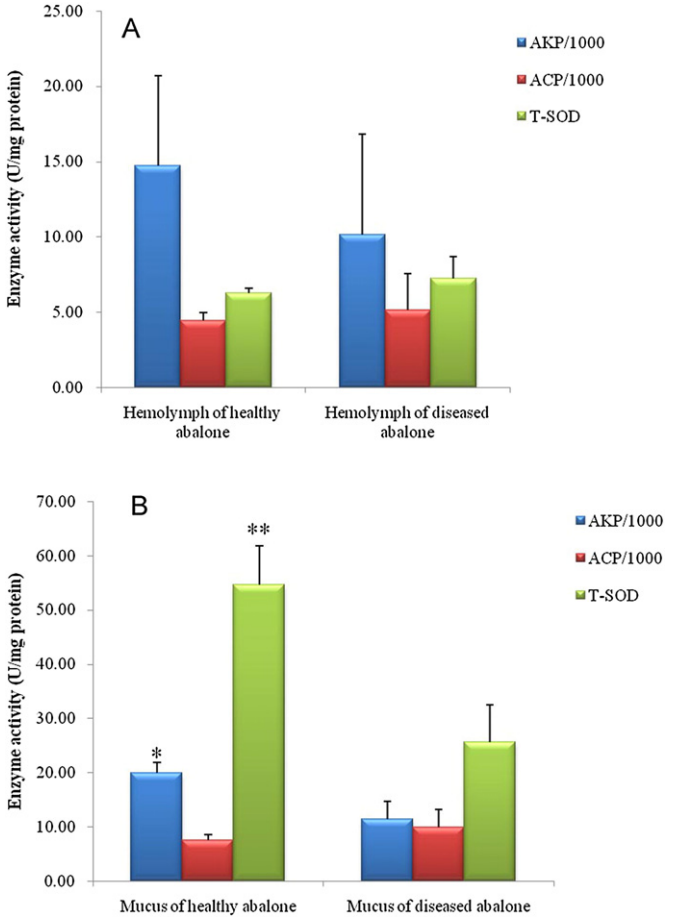

Fig. 2. Comparison of enzyme activities in mucus and haemolymph. Note: *Indicates a significant difference in the same tissue between the control and diseased abalone groups ($p < 0.05$). **Indicates a highly significant difference in the same tissue between the control and diseased abalone groups ($p < 0.01$). Data are presented as mean ± S.D.

ACP activities in the pedal mucus of healthy and diseased abalone were not significantly different. However, in the diseased abalone pedal mucus, activities of AKP and T-SOD were significantly lower compared with the control group ($p < 0.05$ and $p < 0.01$, respectively) (see Fig. 2 B). There was a striking difference between the levels of T-SOD activity in healthy abalone (~50 U/mg) compared with diseased animals (<30 U/mg) ($p < 0.01$).

3.3. Identification of differentially expressed protein sections by SDS-PAGE

Fig. 3 shows the body surface mucus accessions of diseased and normal abalone on the SDS-PAGE electrophoretogram. In the normal abalone, section A and section B were not detected easily; however, in diseased abalone, bands A and B were detected.

Fig. 4 shows the results of protein identification with the MALDI-TOF–TOF spectrum of the trypsinized product from the SDS-PAGE section (Fig. 4). In the MS/MS spectrum, the 10 parent ions were selected for further MS/MS analysis, and the MS/MS spectrum confirmed the responding amino acid sequence by analyzing b- and y-ions derived from the peptide ion. Table 1 shows the MS/MS identification result of section A and section B. Section A was identified as the protein actin, and section B was identified as the protein hemocyanin.

3.4. Identification of differentially expressed protein spots via 2-DE

A total of 16 protein spots were identified using 2-DE gels (see Fig. 5). Differentially expressed proteins were determined and matched to functions or processes using the Gene Ontology database (http://www.uniprot.org/) (Table 2). Most of the differentially expressed proteins were involved in muscle contraction and protein regulation of muscle, energy production and storage, and response to stress.

Contraction and regulation proteins of muscle included actin and troponin I. Actin showed significant downregulation in diseased abalone (spots 7, 8, 10, 13, 15, and 16). Some protein spots were involved in energy production and storage, including fructose-1, 6-bisphosphate aldolase, arginine kinase, and triosephosphate isomerase, with diverse expression patterns in diseased abalone. For stress-responsive proteins, the expression of Cu/Zn-superoxide dismutase (protein spot 6) showed downregulation in diseased abalone.

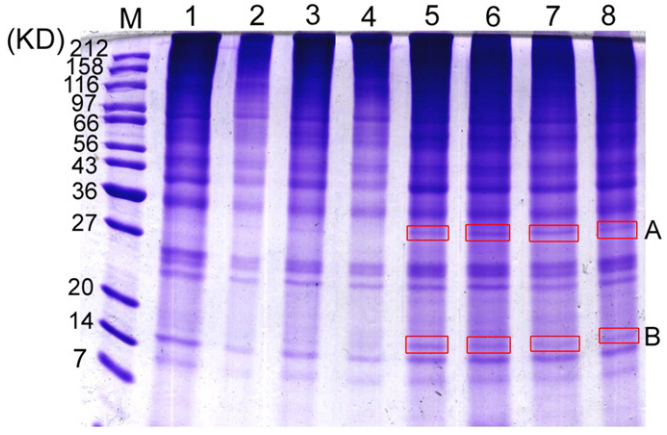

Fig. 3. SDS-PAGE of healthy and diseased abalone pedal surface mucus. Lanes and accessions: The left M lane was used as the molecular weight standard; lanes 1 to 4 represent the pedal mucus of healthy abalone; lanes 5 to 8, pedal mucus of diseased abalone. Sections A, B were significant difference sections. The gel was stained with Coomassie brilliant blue.

4. Discussion

4.1. Ultrastructure pathological changes

Withering syndrome has been associated with temperature, food availability, parasites, and/or bacteria (Gardner et al., 1995; Friedman et al., 1997). Abalone used in the present study had different external symptoms, including atrophied pedal musculature, mantle retraction, epipodial discolorations, and diminished responsiveness to stimuli.

Histopathology is an essential component of investigating disease outbreaks (Hooper et al., 2014). In the present study, electron microscopy of ultrathin sections of healthy muscle tissue revealed tightly arranged and regular structures (see Fig. 1C). Ultrastructure of diseased muscle myofibers appeared hollow and the number of inner intact myofibrils was obviously reduced (see Fig. 1D, F). Microscopically, the myofibers of the foot muscle atrophy and are replaced by connective tissue, presumably due to starvation-induced catabolism (Gardner et al., 1995). Withering syndrome-affected abalones consume less food than healthy abalones (Moore et al., 2001).

The area occupied by digestive/absorptive cells in the digestive gland diminishes, while that occupied by transport duct tissue increases (Gardner et al., 1995; Moore et al., 2001). The degeneration of gastrointestinal tissue in the form of atrophy of tubules increases the amount of connective tissue and inflammation (González et al., 2012). In the present study, the hepatopancreas was damaged most severely; they were full of empty vesicles and devoid of any recognizable cellular structures (see Fig. 1L–N). The number of mitochondria had greatly decreased (Fig. 1M). These morphological changes lead to a loss of functionality of the digestive system, resulting in the animal entering a lethargic state that causes it to catabolize its energy reserves and eventually the structural proteins of its pedal muscles, which are then replaced by connective tissue (Gardner et al., 1995; Braid et al., 2005). These results suggest that infected animals suffer from physical damage to the musculature, and as the infection persists, metabolic homeostasis is compromised, leading to malnourishment and oxidative stress.

The appearance of a novel actin band in the SDS-PAGE gel (Fig. 3) may suggest that actin is degraded or the architecture of the muscle is dismantled due to the disease. The downregulation of actin-associated proteins in the 2-D gels (Fig. 5) may indicate a lack of repair to the diseased tissues or the host is unable to cope with the severity of the infection. Considering that the hepatopancreas was damaged, it is entirely expected that metabolic processes would be altered severely. A reduction in the number of functioning mitochondria is a clear indication of depleted adenosine triphosphate (ATP) stores and/or reduced capacity to generate ATP.

4.2. AKP, ACP, and SOD activity

At present, little information is available regarding the associated effects on the physiological activity of abalones with withering syndrome (Kismohandaka et al., 1993; Rosenblum et al., 2005). ACP and AKP are involved in a variety of metabolic processes such as detoxification, metabolism, and the biosynthesis of macromolecules for various essential functions (Rahman and Siddiqui, 2004). ACP and AKP are both important lysosomal enzymes in marine invertebrates (Liang et al., 2014). Both enzymes play a part in non-specific immunity, participating in degradation of foreign proteins, carbohydrates, and lipids or in phagocytosis (Hu et al., 2015). Interference with either of these 2 enzymes can lead to biochemical impairment of cellular functions and tissue lesions (Enan et al., 1982). Hemolymph ACP and AKP activities in small abalones were induced by injection with *Vibrio parahaemolyticus* (Wang et al., 2004). They can be used as biomarkers for a number of diseases (Samman et al., 1996).

ACP can be altered by the presence of xenobiotics (Rajalakshmi and Mohandas, 2005). ACP plays a role in the killing and digesting of pathogens in immune responses (Cheng and Dougherty, 1989). Research has

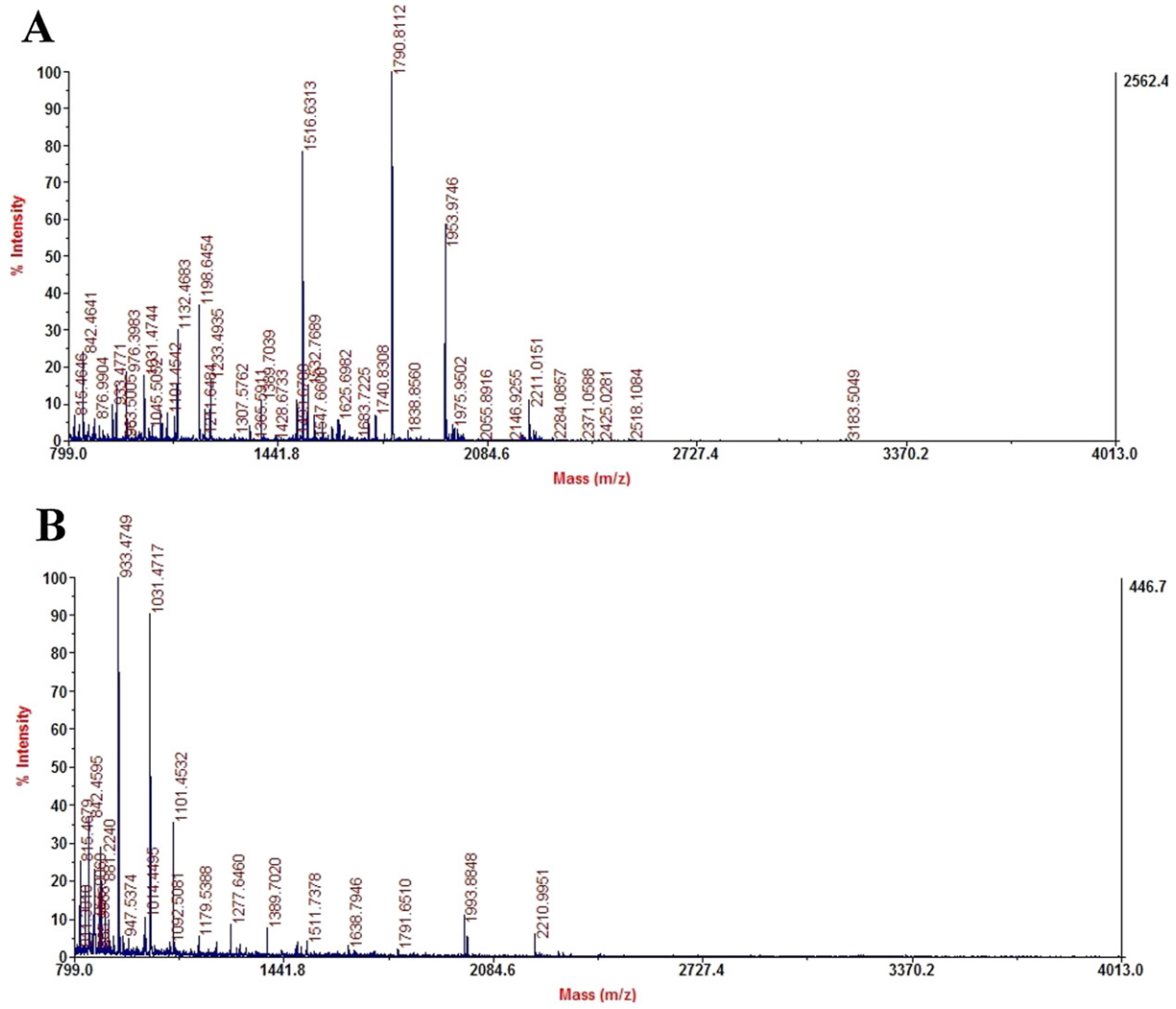

Fig. 4. Identification of actin and hemocyanin proteins with MALDI-TOF–TOF spectrometry of the trypsinized product from SDS-PAGE sections.

shown that serum ACP activity of snails (*Biomphalaria glabrata*) will increase significantly in response to pathogen infection (Cheng and Dougherty, 1989). AKP is a phosphomonoesterase that detoxifies contaminants during normal living conditions (Zhang et al., 2004). In this study, the activities of 2 enzymes (ACP and AKP) were not significantly different between healthy and diseased abalone hemolymph (Fig. 2A). The enzyme activities of ACP in the mucus of healthy and diseased abalone showed few differences ($p > 0.05$); there was a slight increase in ACP in diseased abalone (Fig. 2B). AKP activity declined significantly in the mucus of diseased abalones (Fig. 2B). A decrease in AKP activity but an increase in ACP activity suggested different biochemical regulation mechanisms for ACP and AKP. Together, these results suggest that hydrolases function primarily in the mucus and hemolymph of healthy abalone.

Superoxide dismutase (SOD) is the primary enzyme for defense against ROS-mediated toxicity (Matozzo et al., 2004). SOD catalyzes the dismutation of the superoxide anion to molecular oxygen, and hydrogen peroxide functions as an important component of the antioxidant defense system of the host organism, forming the first line of defense against ROS in the antioxidant pathways (Yang et al., 2010). SOD plays an important role in scavenging free radicals, particularly in defense against oxidization and phagocytosis resulting from stress and cell damage (Yin et al., 2014). In this study, T-SOD enzyme activity in diseased abalone mucus was significantly lower than in healthy abalone ($p < 0.01$). This may indicate that the ability to defend against ROS-mediated toxicity was decreased. In the present study, the hepatopancreas was damaged most severely, with the number of mitochondria greatly decreased (Fig. 1). The mitochondria are the most important sites of ROS production, mitochondria were damaged, this could lead to excess ROS being produced and causes oxidative damage. This was consistent with the reduction of T-SOD enzyme activity in diseased abalone mucus.

Both AKP and T-SOD are involved in detoxification. Reductions in both of these enzymes will have a negative impact on the host. T-SOD

Table 1
Protein identification with MASCOT database searches.

Section	Protein	Species	Accession no	Protein score	Protein score CI%
A	Actin	*Camelus dromedarius*	gi|60389477	635	100
B	Hemocyanin	*Haliotis tuberculata*	gi|12053765	97	99.762

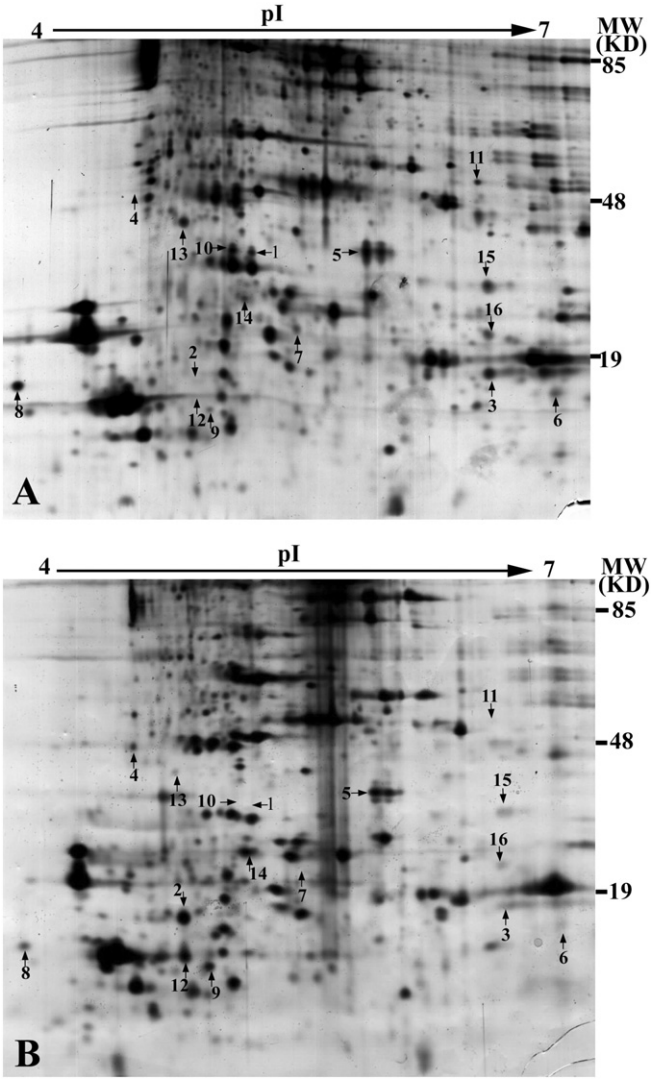

Fig. 5. 2-D gel images of silver-stained proteins (120 μg each load). The spot numbering scheme was based on that described in Table 1. Images of 2-DE from (A) healthy abalone pedal muscle proteins and (B) diseased abalone pedal muscle proteins.

activity was decreased substantially in the mucus of diseased abalone (Fig. 2B) and this was reflected in the downregulation of the enzyme characterized by 2-DE analysis.

4.3. SDS-PAGE bands revealed differences between the pedal surface mucus of normal and diseased abalones

Section A was identified as the protein actin. This suggested that the diseased abalone muscle was damaged; actin was dissolved and flowed out with the surface mucus. Mucus is the first line of defense in molluscs, and the adsorbability of abalone pedals appeared weakened and mucus secretion was reduced in abalones with withering syndrome.

Section B was identified as the protein hemocyanin. The diverse immune functions of hemocyanins in invertebrates have been reviewed recently (Coates and Nairn, 2014). Hemocyanins from both arthropods and molluscs possess antimicrobial and antiviral properties, and are linked to cell death during infection (Coates et al., 2013). The appearance of a hemocyanin fragment (~17 kDa, Fig 3) in diseased abalone suggests a role in immune defense. Abalone hemocyanin displays phenoloxidase activity in response to viral infection (Zhu et al., 2014) and can generate antibacterial fragments in response to sepsis (Zhuang et al., 2015). Furthermore, a number of studies have described increases in hemocyanin mRNA transcript abundance under physiological stress conditions (Zeng et al., 2013). The distinct role of hemocyanin during withering syndrome requires further investigation.

4.4. Identification of differentially expressed protein spots via 2-DE

Contraction and regulation proteins in muscle include actin and troponin I. Thin filaments consist primarily of actin. Troponin, together with the protein tropomyosin, is believed to be the regulatory system for muscle contraction. Six protein spots were identified as actin. The expression level of actin can be related to the rearrangement of both intrachain disulfide bonds (López et al., 2001). Actin showed significant downregulation in diseased abalone. Actin is a ubiquitous eukaryotic structural protein related to the cytoskeleton and muscle. Downregulated actin may be related to atrophied pedal musculature of diseased abalone and degradation during infection. Protein spot 12 was identified as troponin I and showed upregulation in diseased abalone. The regulation of muscle contraction in diseased abalone may be temporarily increased. The combined data of troponin upregulation and actin downregulation indicates that withering syndrome alters the structure of cells, leading to necrosis, muscle atrophy, and altered metabolic capacity. Abalones in this state are more susceptible to infection and predation.

Proteins associated with energy production and storage: We identified several types of proteins associated with energy production and storage including fructose-1,6-bisphosphate aldolase, arginine kinase, and triosephosphate isomerase. Protein spot 11 was identified as fructose-1,6-bisphosphate aldolase, a key enzyme in glycolysis and gluconeogenesis (Table 2 and Fig. 5). Spot 14 was identified as arginine kinase, which plays a crucial role in energy metabolism in invertebrates (Table 2 and Fig. 5). Spot 9 was identified as triosephosphate isomerase, which is involved in the glycolytic process (Table 2 and Fig. 5). The animal enters starvation, which forces it to catabolize its energy reserves and alters the energy balance, with a subsequent decline in foot mass and ultimately death (Friedman et al., 2000; Braid et al., 2005; Moore et al., 2009; González et al., 2012; González et al., 2014).

Proteins associated with stress response: Spot 6 was identified as Cu/Zn superoxide dismutase (Cu/Zn-SOD), which is closely related to immunity in mollusks. It can increase phagocytic cell activity and immune function and protect the cell from ROS poisoning (Kim et al., 2007). The expression of Cu/Zn-superoxide dismutase showed downregulation in diseased abalone. In this study, T-SOD enzyme activity in diseased abalone mucus was significantly lower than in healthy abalone mucus. This result was consistent with the weakened condition of diseased abalone.

4.5. Conclusion

In conclusion, the myofibers of abalones affected by withering syndrome appeared hollow, and the morphology of mitochondria became abnormal. The hepatopancreas was damaged most severely; they were full of empty vesicles and devoid of any recognizable cellular structures. AKP and T-SOD activities in the pedal mucus of diseased abalone were significantly lower than the control group. The differential bands in the SDS-PAGE profiles were identified as actin and hemocyanin. A total of 16 2-DE gel spots were identified; 11 gel spots showed downregulation in diseased abalone. For contraction and regulation proteins of muscle, actin showed significant downregulation. For proteins associated with stress responses, Cu/Zn-superoxide dismutase showed downregulation in diseased abalone. This study describes the pathobiology of abalone suffering with withering syndrome. Future work will focus on the development of biomarkers to detect early signs of this disease in wild and commercial populations.

Table 2
Differentially expressed 2-DE gel protein spots between healthy and diseased abalone muscle identified by MALDI-TOF–TOF.

Spot no[a]	Protein[b]	Species	Accession no	Protein score	Rank result type	Expression quantity in diseased abalone	Molecular function	Biological process	Cellular component
2	Beta-ketoacyl synthase	Frankia sp.CcI3	gi|86741618	64	MS-BLAST	Up-regulated	Acyltransferase, transferase	Fatty acid metabolism, lipid metabolism	Cytoplasm
4	ABC transporter	*Theileria annulata* strain Ankara	gi|84995983	186	MS-BLAST	Up-regulated	ATPase activity, coupled to transmembrane movement of substances, ATP binding	Transport	Membrane
9	Triosephosphate isomerase	*Tenebrio molitor*	gi|22090453	100	Mascot	Up-regulated	Isomerase	Glycolytic process, gluconeogenesis	Cytoplasm
12	Troponin I	*Chlamys nipponensis akazara*	gi|2668408	99.991	Mascot	Up-regulated	Muscle protein	Regulation of muscle contraction	Troponin complex
14	RecName: full = arginine kinase; Short = AK	*Haliotis madaka*	gi|1708614	100	Mascot	Up-regulated	Kinase, transferase	Amino-acid biosynthesis, arginine biosynthesis	Cytoplasm
1	Possible streptogramin lyase, gluconolactonase family	*Nitrosococcus oceani* ATCC 19707	gi|77163812	104	MS-BLAST	Down-regulated	Lyase activity, hydrolase	Ascorbate biosynthesis	Cytoplasm
3	PREDICTED: similar to bromodomain adjacent to zinc finger domain, 1B	*Strongylocentrotus purpuratus*	gi|115945039	134	MS-BLAST	Down-regulated	DNA binding, zinc ion binding	Transcription, transcription regulation	Nucleus
5	PREDICTED: similar to G protein-coupled receptor 112	*Gallus gallus*	gi|118089443	66	MS-BLAST	Down-regulated	G-protein coupled receptor, receptor, transducer	G-protein coupled receptor signaling pathway	Membrane
6	Cu/Zn-superoxide dismutase	*Haliotis diversicolor*	gi|166406955	99.547	Mascot	Down-regulated	Oxidoreductase	Metal ion binding/oxidation reduction, superoxide	Cytoplasm
11	Fructose 1,6-bisphosphate aldolase	*Haliotis diversicolor*	gi|166406769	100	Mascot	Down-regulated	Lyase	Glycolysis	Cytosol, mitochondrion
7	Actin-2	*Lotharella amoeboformis*	gi|15216717	99.48	Mascot	Down-regulated	ATP binding	ATP binding, protein binding	Cytoplasm, cytoskeleton
8	Beta-actin	*Blaptica dubia*	gi|213032429	97.88	Mascot	Down-regulated	ATP binding	ATP binding, protein binding	Cytoplasm, cytoskeleton
10	Actin 88F	*Drosophila mauritiana*	gi|294714383	100	Mascot	Down-regulated	ATP binding	ATP binding, protein binding	Cytoplasm, cytoskeleton
13	Actin-2	*Culex quinquefasciatus*	gi|170038869	100	Mascot	Down-regulated	ATP binding	ATP binding, protein binding	Cytoplasm, cytoskeleton
15	Beta-actin	*Astronotus ocellatus*	gi|182623856	100	Mascot	Down-regulated	ATP binding	ATP binding, protein binding	Cytoplasm, cytoskeleton
16	Actin-2	*Culex quinquefasciatus*	gi|170038869	100	Mascot	Down-regulated	ATP binding	ATP binding, protein binding	Cytoplasm, cytoskeleton

[a] Spot number corresponds to the number on the 2-DE in Fig. 5.
[b] Protein identified by *de novo* sequencing and MASCOT (www.matrixscience.com) from the NCBI nonredundant data.

Acknowledgements

This study was funded by NSFC (No. U1205121), Hi-Tech Research and Development (863) Program of China (No. 2012AA10A412) and the Earmarked Fund for Modern Agro-industry Technology Research System (No. CARS-48), Key Funds for the Development of Marine Hi-tech Industry in Fujian Province [No. 16(2013)]. It was also supported by the Program for Innovative Research Team (in Science and Technology) in University of Henan Province (15IRTSTHN018), Henan Basic and Advanced Research Program (No. 152300410206), Henan Science and Technology Program (No. 14B240003), and the PhD Start-up Fund of Henan Normal University (No. qd13053), the Training Program of the National Natural Science Foundation of Henan Normal University.

References

Balseiro, P., Aranguren, R., Gestal, C., Novoa, B., Figueras, A., 2006. *Candidatus Xenohaliotis californiensis* and *Haplosporidium montforti* associated with mortalities of abalone *Haliotis tuberculata* cultured in Europe. Aquaculture 258, 63–72.

Braid, B., Moore, J., Robbins, T., Hedrick, R., Tjeerdema, R., Friedman, C., 2005. Health and survival of red abalone, *Haliotis rufescens*, under varying temperature, food supply, and exposure to the agent of whithering syndrome. J. Invertebr. Pathol. 89, 219–231.

Cai, J.P., Wang, Z.X., 2008. Characterization and identification of virulent *Klebsiella oxytoca* isolated from abalone (*Haliotis diversicolor supertexta*) postlarvae with mass mortality in Fujian, China. J. Invertebr. Pathol. 97, 70–75.

Cheng, T., Dougherty, W., 1989. Ultrastructural evidence for the destruction of *Schistosoma mansoni* sporocysts associated with elevated lysosomal enzyme levels in *Biomphalaria glabrata*. J. Parasitol. 75, 928–941.

Coates, C.J., Nairn, J., 2014. Diverse immune functions of hemocyanins. Dev. Comp. Immunol. 45 (1), 43–55.

Coates, C.J., Whalley, T., Wyman, M., Nairn, J., 2013. A putative link between phagocytosis-induced apoptosis and hemocyanin-derived phenoloxidase activation. Apoptosis 18, 1319–1331.

Crosson, L.M., Wight, N., VanBlaricom, G.R., Kiryu, I., Moore, J.D., Friedman, C.S., 2014. Abalone withering syndrome: distribution, impacts, current diagnostic methods and new findings. Dis. Aquat. Org. 108, 261–270.

Di, G., Luo, X., You, W., Zhao, J., Kong, X., Ke, C., 2015. Proteomic analysis of muscle between hybrid abalone and parental lines *Haliotis gigantea* Reeve and *Haliotis discus hannai* Ino. Heredity 114 (6), 564–574.

Di, G., You, W., Yu, J., Wang, D., Ke, C., 2013. Genetic changes in muscle protein following hybridization between *Haliotis diversicolor* reeve Japan and Taiwan populations revealed using a proteomic approach. Proteomics 13, 845–859.

Enan, E.E., Enan, O.H., El-Sebae, A.E., 1982. Biochemical target affected by sub-lethal doses of organophosphorus insecticides. Int. Pest Control 24, 120–122.

Friedman, C.S., Andree, K.B., Beauchamp, K.A., Moore, J.D., Robbins, T.T., Shields, J.D., Hedrick, R.P., 2000. "*Candidatus Xenohaliotis californiensis*" a newly described pathogen of abalone, Haliotis spp, along the West Coast of North America. Int. J. Syst. Evol. Microbiol. 50, 847–855.

Friedman, C.S., Biggs, W., Shields, J.D., Hedrick, R.P., 2002. Transmission of withering syndrome in black abalone, *Haliotis cracherodii* Leach. J. Shellfish Res. 21 (2), 817–824.

Friedman, C.S., Grindley, R., Keogh, J.A., 1997. Isolation of a fungus fromshell lesions of New Zealand abalone, *Haliotis iris* Martyn and *H. australis* Gmelin. Molluscan Res. 18, 313–324.

Friedman, C.S., Wight, N., Crosson, L.M., White, S.J., Strenge, R.M., 2014. Validation of a quantitative PCR assay for detection and quantification of "*Candidatus Xenohaliotis californiensis*". Dis. Aquat. Org. 108, 251–259.

Gardner, G.R., Harshbarger, J.C., Lake, J.L., Sawyer, T.K., Price, K.L., Stephenson, M.D., Haaker, P.L., Togstad, H.A., 1995. Association of prokaryotes with symptomatic appearance of withering syndrome in black abalone *Haliotis cracheroddi*. J. Invertebr. Pathol. 66, 111–120.

González, R.C., Brokordt, K., Lohrmann, K.B., 2012. Physiological performance of juvenile *Haliotis rufescens* and *Haliotis discus hannai* abalone exposed to the withering syndrome agent. J. Invertebr. Pathol. 111 (1), 20–26.

González, R., Lohrmann, K.B., Pizarro, J., Brokordt, K., 2014. Differential susceptibility to the withering syndrome agent and renal coccidia in juvenile *Haliotis rufescens*, *Haliotis discus hannai* and the interspecific hybrid. J. Invertebr. Pathol. 116, 13–17.

Hooper, C., Day, R., Slocombe, R., Benkendorff, K., Handlinger, J., Goulias, J., 2014. Effects of severe heat stress on immune function, biochemistry and histopathology in farmed Australian abalone (hybrid *Haliotis laevigata* × *Haliotis rubra*). Aquaculture 432, 26–37.

Hu, M., Li, L., Sui, Y., Li, J., Wang, Y., Lu, W., Dupont, S., 2015. Effect of pH and temperature on antioxidant responses of the thick shell mussel *Mytilus coruscus*. Fish Shellfish Immunol. 46, 573–583.

Jiang, J.Z., Zhu, Z.N., Zhang, H., Liang, Y.Y., Guo, Z.X., Liu, G.F., Su, Y.L., Wang, J.Y., 2012. Quantitative PCR detection for abalone shriveling syndrome-associated virus. J. Virol. Methods 184 (1), 15–20.

Kim, K.Y., Lee, S.Y., Cho, Y.S., Bang, I.C., Kim, K.H., Kim, D.S., Nam, Y.K., 2007. Molecular characterization and mRNA expression during metal exposure and thermal stress of copper/zinc- and manganese-superoxide dismutases in disk abalone, *Haliotis discus discus*. Fish Shellfish Immunol. 23, 1043–1059.

Kismohandaka, G., Friedman, C., Roberts, W., Hedrick, R., Crosby, M., 1993. Investigation of physiological parameters of black abalone with withering syndrome. J. Shellfish Res. 12, 131–132.

Li, W.J., Yan, Z.L., 2010. Establishment of an ecological mode for abalone aquaculture. S. China Fish. Sci. 6, 54–59.

Liang, S., Luo, X., You, W., Luo, L., Ke, C., 2014. The role of hybridization in improving the immune response and thermal tolerance of abalone. Fish Shellfish Immunol. 39 (1), 69–77.

López, J.L., Mosquera, E., Fuentes, J., Marina, A., Vázquez, J., Alvarez, G., 2001. Two-dimensional gel electrophoresis of *Mytilus galloprovincialis*: differences in protein expression between intertidal and cultured mussels. Mar. Ecol. Prog. Ser. 224, 149–156.

Matozzo, V., Ballarin, L., Marin, M.G., 2004. Exposure of the clam *Tapes philippinarum* to 4-nonylphenol: changes in antioxidant enzyme activities and re-burrowing capability. Mar. Pollut. Bull. 48, 563–571.

Moore, J., Cherr, G., Friedman, C., 2001. Detection of *Candidatus Xenohaliotis californiensis* (*Rickettsiales*-like prokaryote) inclusions in tissue squashes of abalone (Haliotis spp.) gastrointestinal epithelium using a nucleic acid fluorochrome. Dis. Aquat. Org. 46, 147–152.

Moore, J., Juhasz, C., Robbins, T., Vilchis, I., 2009. Green abalone, *Haliotis fulgens* infected with the agent of withering syndrome do not express disease signs under a temperature regime permissive for red abalone, *Haliotis rufescens*. Mar. Biol. 156, 2325–2330.

Rahman, M.F., Siddiqui, M.K., 2004. Biochemical effects of vepacide (from *Azadirachta indica*) on Wistar rats during subchronic exposure. Ecotoxicol. Environ. Saf. 59, 332–339.

Rajalakshmi, S., Mohandas, A., 2005. Copper-induced changes in tissue enzyme activity in a freshwater mussel. Ecotoxicol. Environ. Saf. 62, 140–143.

Rosenblum, E.S., Robbins, T.T., Scott, B.B., Nelson, S., Juhasz, C., Craigmill, A., Tjeerdema, R.S., Moore, J.D., Friedman, C.S., 2008. Efficacy, tissue distribution, and residue depletion of oxytetracycline in WS-RLP infected California red abalone *Haliotis rufescens*. Aquaculture 277, 138–148.

Rosenblum, M., Viant, B., Braid, J., Moore, J., Friedman, C., Tjeerdema, R., 2005. Characterizing the metabolic actions of natural stresses in the California red abalone, *Haliotis rufescens* using 1 H NMR metabolomics. Metabolomics 1, 199–209.

Samman, S., Soto, C., Cooke, L., Ahmad, Z., Farmakalidis, E., 1996. Is erythrocyte alkaline phosphatase activity a marker of zinc status in humans? Biol. Trace.Elem. Res. 51, 285–291.

Wang, D.Z., Li, C., Xie, Z.X., Dong, H.P., Lin, L., Hong, H.S., 2011. Homology-driven proteomics of dinoflagellates with unsequenced genomes using MALDI-TOF/TOF and automated de novo sequencing. Evid. Based Complement. Alternat. Med. http://dx.doi.org/10.1155/2011/471020.

Wang, S.H., Wang, Y.L., Zhang, Z.X., 2004. Different response of innate immune factors in abalone *Haliotis diversicolor supertexta* to E. coli or *Vibrio parahaemolyticus* infection. J. Shellfish Res. 23, 1173–1177.

Wetchateng, T., Friedman, C., Wight, N., Lee, P., Teng, P., Sriurairattana, S., Wongprasert, K., Withyachumnarnkul, B., 2010. Withering syndrome in the abalone *Haliotis diversicolor supertexta*. Dis. Aquat. Org. 90, 69–76.

Yang, S.P., Wu, Z.H., Jian, J.C., Zhang, X.Z., 2010. Effect of marine red yeast *Rhodosporidium paludigenum* on growth and antioxidant competence of *Litopenaeus vannamei*. Aquaculture 309, 62–65.

Yin, F., Dan, X.M., Sun, P., Shi, Z.H., Gao, Q.X., Peng, S.M., Li, A.X., 2014. Growth, feed intake and immune responses of orange-spots grouper (*Epinephelus coioides*) exposed to low infectious doses of ectoparasite (*Cryptocaryon irritans*). Fish Shellfish Immunol. 36 (1), 291–298.

Zeng, D., Chen, X., Xie, D., Zhao, Y., Yang, C., Li, Y., 2013. Transcriptome analysis of Pacific white shrimp (*Litopenaeus vannamei*) hepatopancreas in response to Taura Syndrome Virus (TSV) experimental infection. PLoS ONE 8, e57515.

Zhang, M., Wang, L., Guo, Z.Y., Wang, B.J., 2004. Effect of lipopolysaccharide and *Vibrio anguillarum* on the activities of phosphatase, superoxide dismutase and the content of hemocyanin in the serum of *Fenneropenaeus chinensis*. Mar. Sci. 28, 22–25.

Zhu, H., Zhuang, J., Feng, H., Liang, R., Wang, J., Xie, L., Zhu, P., 2014. Cryo-EM structure of isomeric molluscan hemocyanin triggered by viral infection. PLoS ONE 9, e98766.

Zhuang, J., Cai, G.Q., Lin, Q.Y., Wu, Z.J., Xie, L.H., 2010. A bacteriophage-related chimeric marine virus infecting abalone. PLoS ONE 5, 1–12.

Zhuang, J., Coates, C.J., Zhu, H., Zhu, P., Wu, Z., Xie, L., 2015. Identification of candidate antimicrobial peptides derived from abalone hemocyanin. Dev. Comp. Immunol. 49, 96–102.